

## Efficient photocatalytic activity with carbon-doped SiO<sub>2</sub> nanoparticles

Cite this: *Nanoscale*, 2013, 5, 6167

Dongen Zhang,<sup>ac</sup> Jinbo Wu,<sup>a</sup> Bingpu Zhou,<sup>b</sup> Yaying Hong,<sup>a</sup> Shunbo Li<sup>a</sup> and Weijia Wen<sup>\*a</sup>

Photocatalysis provides a 'green' approach to completely eliminate various kinds of contaminants that are fatal for current environmental and energy issues. Semiconductors are one of the most frequently used photocatalysts as they can absorb light over a wide spectral range. However, it is also well known that naked SiO<sub>2</sub> is not an efficient photocatalyst due to its relatively large band gap, which could only absorb shortwave ultraviolet light. In this report, nanoscale particles of carbon-doped silicon dioxide (C-doped SiO<sub>2</sub>) for use in photocatalysis were successfully prepared by a facile one-pot thermal process using tetraethylorthosilicate (TEOS) as the source of both silicon and carbon. These particles were subsequently characterized by thermogravimetric analysis, X-ray diffraction, standard and high resolution transmission electron microscopy and X-ray photoelectron spectroscopy. The C-doped SiO<sub>2</sub> displayed outstanding photocatalytic properties, as evidenced by its catalysis of Rhodamine B degradation under near-UV irradiation. We propose that carbon doping of the SiO<sub>2</sub> lattice creates new energy states between the bottom of the conduction band and the top of the valence band, which narrows the band gap of the material. As a result, the C-doped SiO<sub>2</sub> nanoparticles exhibit excellent photocatalytic activities in a neutral environment. The novel synthesis reported herein for this material is both energy efficient and environmentally friendly and as such shows promise as a technique for low-cost, readily scalable industrial production.

Received 17th March 2013

Accepted 28th April 2013

DOI: 10.1039/c3nr01314f

[www.rsc.org/nanoscale](http://www.rsc.org/nanoscale)

### Introduction

Dye pollutant discharges resulting from industrial operations are currently a significant source of environmental contamination. Over the past several decades, various physical, chemical, and biological techniques for the decolorization of dye effluents have been developed. Conventional treatments such as coagulation,<sup>1–3</sup> flocculation,<sup>4</sup> adsorption,<sup>5</sup> ultrafiltration,<sup>6</sup> reverse osmosis<sup>7</sup> and membrane technologies,<sup>8</sup> however, merely transfer the dye from the liquid to the solid phase, necessitating further treatment and leading to secondary pollution.<sup>9</sup> Destructive techniques such as chemical oxidation and advanced oxidation processes (AOPs) may mitigate these problems, but still suffer from high costs and incomplete degradation.<sup>10</sup> Among the AOPs, photocatalysis is arguably one of the most efficient methods. Photocatalysis is a process by which a semiconductor material absorbs light of energy greater than or equal to its band gap, resulting in the excitation of valence

electrons to the conduction band. Such charge separation leads to the formation of electron–hole pairs which may react with hydroxyl groups and oxygen molecules adsorbed on the surface of the catalyst, generating hydroxyl radicals and superoxide radical ions, respectively, both of which are highly reactive and can readily oxidize organic compounds.<sup>10,11</sup>

Photocatalysis has several advantages over other processes. It is cost-effective, may use ultraviolet (UV), near-UV or solar light as an energy source, may operate at or near room temperature, has no requirement for the addition of other chemicals, is able to efficiently mineralize most organic compounds and can be readily implemented in conjunction with other conventional technologies to form hybrid systems.<sup>12</sup> As a result of these benefits, photocatalytic processes have, in recent years, received significant attention and are considered as promising advanced oxidation technologies for environmental remediation.<sup>13–20</sup> Photocatalysts used in ultraviolet (UV) light-activated processes are semiconductor materials such as TiO<sub>2</sub>, ZnO, Al<sub>2</sub>O<sub>3</sub> and MgO.<sup>21</sup> Despite their remarkable features, there exist certain associated drawbacks such as faster charge carrier recombination, low photo-induced reaction efficiency and rapid deactivation due to the accumulation of less reactive by-products on the photocatalyst's surface.<sup>22</sup> In this regard, development of non-TiO<sub>2</sub>-based nanomaterials as efficient photocatalysts was explored. Consequently, from an application

<sup>a</sup>Department of Physics and KAUST-HKUST Micro/Nanofluidic Joint Laboratory, The Hong Kong University of Science and Technology, Clear Water Bay, Kowloon, Hong Kong. E-mail: [phwen@ust.hk](mailto:phwen@ust.hk); Fax: +852 2358 1652; Tel: +852 2358 7979

<sup>b</sup>Nano Science and Technology Program, The Hong Kong University of Science and Technology, Clear Water Bay, Kowloon, Hong Kong

<sup>c</sup>Department of Chemical Engineering, Huaihai Institute of Technology, No.59 Cangwu Road, Lianyungang 222005, P.R. China

point of view, choosing a material with an appropriate surface area, particle size, porosity and band gap will dramatically improve its photocatalytic activity.<sup>23</sup>

To date, various oxide, sulfide and oxynitride semiconductor materials have been investigated for use as photocatalysts,<sup>24–26</sup> the exception being SiO<sub>2</sub>, which has not been considered owing to its wider band gap that only absorbs shortwave ultraviolet light (<300 nm).<sup>27</sup> SiO<sub>2</sub> appears only rarely to have been used as a photocatalyst on its own,<sup>28–30</sup> although numerous reports on the preparation of SiO<sub>2</sub>-based composites for use in the photocatalytic degradation of dyes appear in the literature. In these instances, SiO<sub>2</sub> is generally added to the composite as a support material to enhance the thermal stability of the photocatalyst and to increase its surface acidity, which is an efficient means of improving catalytic activity.<sup>31–33</sup> To date, however, the non-metal doping of SiO<sub>2</sub> materials for the photocatalytic degradation of dyes has not been reported.

In this report, we present a new class of stable, efficient and environmentally friendly C-doped SiO<sub>2</sub> photocatalysts, prepared *via* the thermal decomposition of tetraethylorthosilicate (TEOS) through a facile, reproducible, one-pot synthetic method. The activity of these materials has been carefully evaluated by studying the photocatalytic decomposition of Rhodamine B (RhB) in aqueous solution under near-UV-light illumination. The results show that these novel photocatalysts display excellent photocatalytic activity as a consequence of new energy states generated between the bottom of the conduction band and the top of the valence band resulting from C doping of SiO<sub>2</sub>.

## Methods

### Sample preparation

All chemicals used in this study were of analytical grade and were used as-received without further purification. In a typical synthesis, tetraethylorthosilicate (TEOS, Janssen Chimica, 99%, 0.5 mL), oleic acid (Aldrich, 90%, 1 mL), oleylamine (Aldrich, 70%, 1 mL), and octadecene (Aldrich 90%, 4 mL) were mixed using a magnetic stirrer, after which the mixture was heated gradually to 260 °C, and held at that temperature for 2 h. The resulting yellowish solution was then cooled to room temperature and ethanol (Scharlau, 99.9%, 40 mL) was added with continuous stirring, forming a yellow precipitate which was separated *via* centrifugation. The precipitate was subsequently dissolved in cyclohexane and again centrifuged to remove any insoluble material. The cyclohexane solution was evaporated to dryness overnight at 40 °C and the resulting dry powder was calcined at 600 °C for 2 h. For comparison, a control sample (denoted as pure SiO<sub>2</sub>) was prepared: TEOS (3 mL) was added dropwise to a mixed solution of ethanol (16 mL) and ammonia (28%, 2 mL) at 60 °C under magnetic stirring. After the addition of TEOS, the clear solution gradually turned opaque owing to the formation of a white precipitate. After continuous stirring for 2 h, the white precipitate was filtered. The products were repeatedly washed with water and ethanol four times, then dried in a vacuum oven at 80 °C for 4 h, finally calcined at 600 °C for 2.5 h in a muffle furnace.

### Characterization

The calcined products were characterized by TEM and HRTEM using JEOL 2010 and 2010F microscopes at an accelerating voltage of 200 kV. Samples for TEM measurements were prepared by sonicating the calcined product in ethanol for 30 min and evaporating a drop of the resulting suspension onto a carbon-coated Holey film supported on a copper grid. An energy-dispersive X-ray spectrometer was attached to the JEOL 2010F and XRD analyses were performed using a Philips PW-1830 X-ray diffractometer with Cu K $\alpha$  radiation ( $\lambda = 1.5406 \text{ \AA}$ ) at a scanning speed of  $5^\circ \text{ min}^{-1}$  over the  $2\theta$  range of  $10\text{--}50^\circ$ . The XPS spectra were measured on a Perkin-Elmer model PHI 5600 XPS system with a resolution of 0.3–0.5 eV using a monochromated aluminum anode X-ray source with K $\alpha$  radiation (1486.6 eV). The samples were dispersed on a carbon tape attached to the sample holder. The binding energies of the Si 2p, O 1s and C 1s peaks from samples were calibrated with respect to the C 1s peak from the carbon tape at 285 eV.

### Photocatalysis measurements

To analyze the photocatalytic activity, RhB was dissolved in distilled water at a concentration of 0.1 mM. Prior to irradiation, 2 mg of the photocatalyst were mixed with 5 mL of the RhB solution in a 10 mL beaker and the beaker was covered. The suspension was then illuminated with a Dymax near-UV Curing Lamp System with the radiation centered at 365 nm. The light intensity at the center of the beaker was measured at approximately  $70 \text{ mW cm}^{-2}$  using a photometer (ABM Model 150). During irradiation, the suspension was magnetically stirred and maintained at room temperature. Following irradiation, suspension aliquots of approximately 2 mL were taken and centrifuged at  $14\,000 \text{ rpm min}^{-1}$  for 5 min. The total organic carbon (TOC) was measured with a Shimadzu TOC-Vcph analyzer. The dye concentration in the resulting solution was then measured by determining the RhB absorption intensity using a PerkinElmer Lambda 20 UV/Vis spectrometer.

## Results and discussion

Fig. 1(a) shows the X-ray diffraction (XRD) pattern of the synthesized material. The amorphous nature of the SiO<sub>2</sub> within the product is evident by the broad peak at approximately  $15\text{--}30^\circ 2\theta$ ,<sup>34</sup> and is further confirmed by the energy-dispersive X-ray spectroscopy (EDX) spectrum (Fig. 1(b)), which indicates that, apart from traces of Cu and C resulting from the transmission electron microscopy (TEM) grid, only Si and O are present. The chemical binding states of the SiO<sub>2</sub> were investigated by X-ray photoelectron spectroscopy (XPS). The two major peaks identified at 103.3 and 532.8 eV are shown in Fig. 1(c) and (d) respectively, and correspond to the binding energies of Si 2p and O 1s.<sup>35,36</sup> The XPS data indicate that Si and O atoms are present in the ratio of 1 : 2, providing further evidence that the synthesized material is SiO<sub>2</sub>. The microstructure of the material was examined *via* both TEM and high resolution TEM (HRTEM) and the images obtained are shown in Fig. 1(e) and (f). The TEM image clearly shows that the SiO<sub>2</sub> nanoparticles have a typical

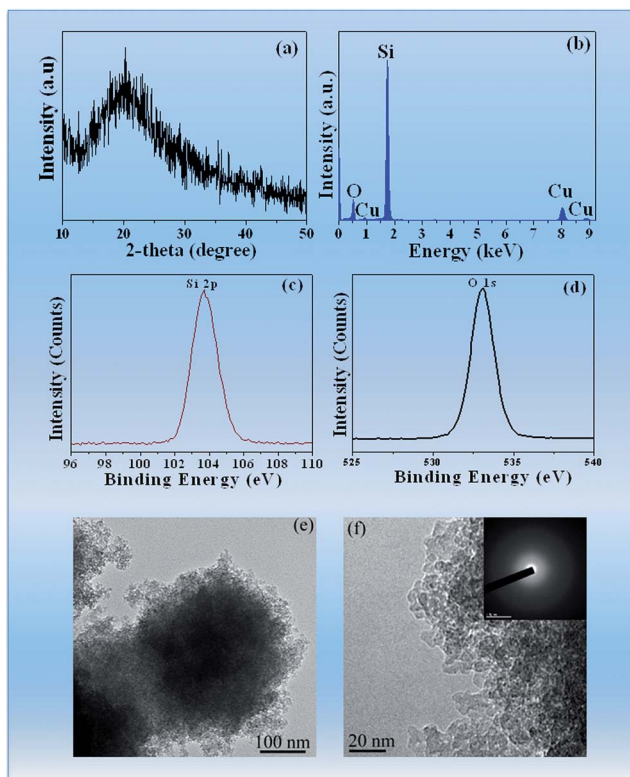


**Fig. 1** (a) XRD pattern, (b) EDS spectra, (c) Si 2p and (d) O 1s XPS spectra, (e) low-magnification TEM image and (f) HRTEM image (with the corresponding SAED pattern, inset) of a synthesized SiO<sub>2</sub> sample.

mesoporous structure and that the average particle size may be estimated at approximately 20 to 30 nm. The mesopores between nanoparticles will allow light scattering inside their pore channels and thus enhance the light harvesting efficiency of this material. The HRTEM image of the sample demonstrates that the sample is entirely amorphous with no crystalline core, as confirmed by its electron diffraction pattern (inset).<sup>37</sup> Furthermore, the mesoporous SiO<sub>2</sub> has a three dimensionally interconnected and disordered globular-like mesopore structure and the size of mesopore is almost homogeneous, which is similar to the MSU mesoporous silica as discussed elsewhere.<sup>38,39</sup>

The photocatalytic decomposition of RhB in aqueous solution under UV irradiation and in the presence of the synthesized SiO<sub>2</sub> material was subsequently evaluated. Fig. 2(a) shows the UV/vis spectra of the RhB–SiO<sub>2</sub> solution both before irradiation and at regular intervals during near-UV irradiation ( $\lambda = 365$  nm) up to 3.5 h. It can be seen that the characteristic absorption band of RhB at 554 nm decreases significantly with increasing irradiation and has essentially completely disappeared after approximately 330 min. The blue shift of the absorption band following prolonged irradiation is attributed to the stepwise deethylation of RhB. In this process, the ethyl groups of the tetraethylated RhB molecule are removed one at a time, resulting in *N,N,N'*-triethylated rhodamine with absorption at 539 nm, *N,N'*-diethylated rhodamine (522 nm) and *N*-ethylated rhodamine (510 nm).<sup>40,41</sup> Concurrent with the irradiation, the color of

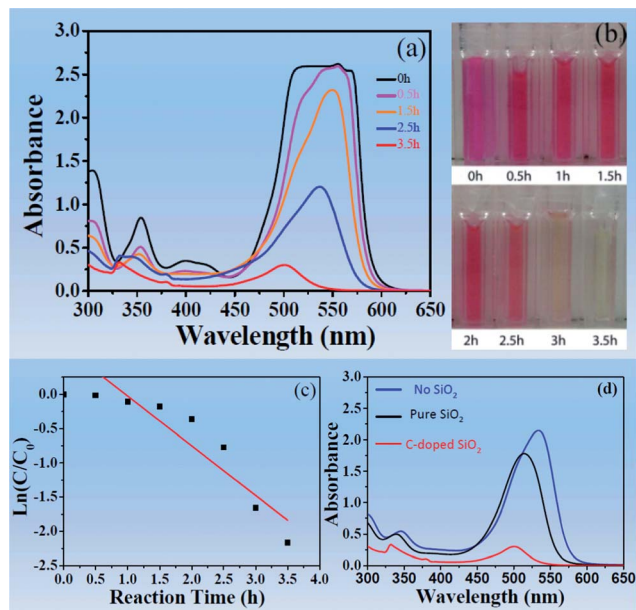


**Fig. 2** (a) UV-vis absorption spectra and (b) photograph of RhB solutions before and after irradiation, using SiO<sub>2</sub> prepared at 260 °C; (c) kinetics of degradation; (d) comparison of photocatalytic degradation of RhB with pure SiO<sub>2</sub> and C-doped SiO<sub>2</sub> as catalysts by irradiation for 3.5 h. The original concentration of RhB is 0.1 mM.

the RhB solution changes from its initial pink/red to a transparent light yellow, as shown in Fig. 2(b). In addition, the TOC value of the dye decreased about 86% after 3 h of irradiation, which indicates that the RhB mineralization by the C-doped SiO<sub>2</sub> photocatalyst is possible. Fig. 2(c) shows the  $\ln(C/C_0)$  versus reaction time curve of the photocatalytic degradation of RhB over C-doped SiO<sub>2</sub> catalysts. The kinetic data of the photocatalytic degradation approximately fit to the apparent first-order reaction kinetics after irradiation for 0.5 h and the reaction rate constant ( $-\kappa$ ) calculated from the slope of the curve is  $0.8351 \text{ h}^{-1}$ . Fig. 2(d) also shows the degradation rates of RhB over different samples. We can see that the synthesized SiO<sub>2</sub> exhibits higher photocatalytic activities than pure SiO<sub>2</sub>. These results clearly demonstrate that RhB bleaching occurs mainly *via* the destruction of the molecule's aromatic structure and that the synthesized SiO<sub>2</sub> has demonstrated substantial photocatalytic activity.

Based on photocatalytic theory, we have developed a proposed reaction mechanism for the SiO<sub>2</sub>-catalyzed photo-degradation of aqueous RhB. In our work, the process used for the synthesis of SiO<sub>2</sub> employed solely organic reagents, and thus all reactions were carried out under anhydrous conditions, where TEOS will produce both silica and various organic compounds. These organic groups may then decompose on heating to form Si–O–C structures and create substitutional carbon defects for Si.<sup>42,43</sup> Similar forms of carbon doping have been shown to reduce the band gap of catalysts such as TiO<sub>2</sub> and ZnO.<sup>44,45</sup> The UV/Vis absorption spectrum of the C-doped SiO<sub>2</sub> displays a red shift as compared with the spectrum of pure SiO<sub>2</sub>, as reported by Sailor *et al.*<sup>43</sup> Therefore, the band gap (3.28 eV, Fig. 3(a)) of the SiO<sub>2</sub> synthesized in this study is likely

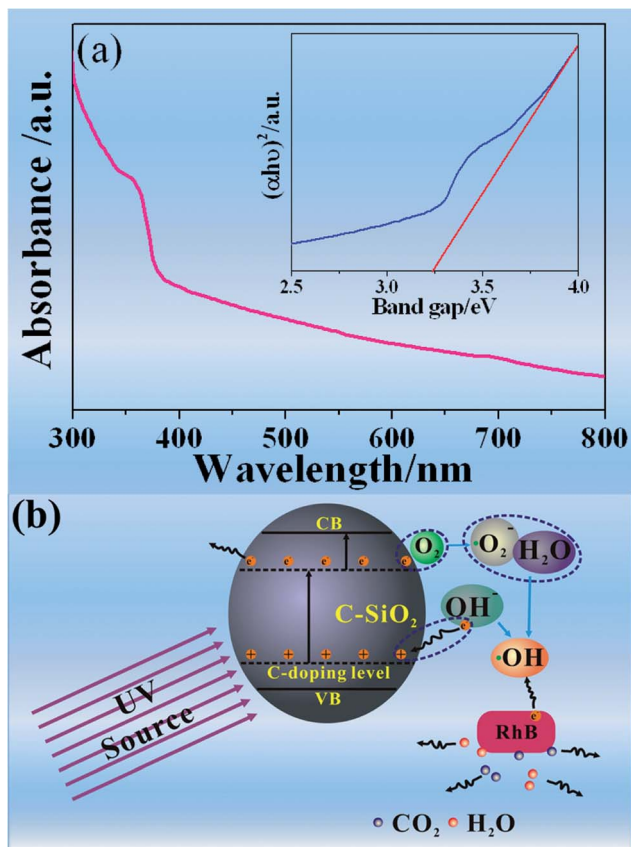


Fig. 3 Proposed photocatalytic mechanism over the C-doped SiO<sub>2</sub> nanoparticles.

reduced because of the carbon doping according to the K-M model, such that new energy states are created between the bottom of the conduction band and the top of the valence band. When the synthesized SiO<sub>2</sub> is used as a photocatalyst, it is capable of simultaneous adsorption/absorption of both the reactants (the organic substrates and dissolved dioxygen) and the requisite light energy. Fig. 3(b) shows the illustration of the basic photocatalytic process, in which excited electrons generated by absorption of near-UV-light are first transferred to the defect level, then they absorb additional energy less than that of the first excitation to transfer to the conduction band, with the formation of the excited-state species SiO<sub>2</sub>\*. This excited-state species is a more powerful redox reactant than normal SiO<sub>2</sub> as a result of the formation of electron-hole pairs, and the holes and electrons in the SiO<sub>2</sub>\* subsequently react with OH<sup>-</sup> and O<sub>2</sub> molecules on the catalyst surface to form 'OH radicals and superoxide anion radicals (O<sub>2</sub><sup>•-</sup>), respectively. The O<sub>2</sub><sup>•-</sup> radicals then interact with adsorbed H<sub>2</sub>O to produce more 'OH radicals, which are known to be a powerful oxidizing species, which then react with the RhB molecule to degrade it.<sup>46</sup> As the decomposition of the dye progresses, the adsorption equilibrium is shifted and more RhB can move from solution to the catalyst interface where it is subsequently decomposed. This proposed mechanism is partly based on several published studies concerning the generation of 'OH radicals during photolysis in aqueous TiO<sub>2</sub> solutions.<sup>47–49</sup>

To clarify the origin of the aforementioned spectral absorption shift observed for the synthesized SiO<sub>2</sub> prepared at 260 °C as compared with pure SiO<sub>2</sub>, XPS analysis was carried out to elucidate the material's surface chemical composition and electronic states. The broad-range XPS spectrum shown in Fig. 4(a) confirms that the synthesized SiO<sub>2</sub> contains C in addition to Si and O. Fig. 4(b) shows the high-resolution XPS spectra of the C 1s region for the SiO<sub>2</sub>, which exhibit three contributing peaks. The first main peak at 284.8 eV is attributed to the residual C from the synthesis as well as adventitious hydrocarbons from the XPS instrument itself. The second peak at 286.7 eV is attributed to Si-O-C groups in the material, while the last peak at 288.6 eV is due to carbonate or carbon dioxide adsorbed on the SiO<sub>2</sub> surface.<sup>45</sup> From this we conclude that lattice C-doping is responsible for the observed red-shift in the SiO<sub>2</sub> absorption edge and its enhanced near-UV-light absorption.

The effects of the temperature applied in the synthesis reaction on the catalytic activity of the resulting C-doped SiO<sub>2</sub> during the photodegradation of RhB are shown in Fig. 5. From these plots it is evident that, as the reaction temperature is increased from 150 to 280 °C, the photocatalytic activity first increases and then decreases, and the maximum activity is associated with a reaction temperature of 260 °C. It is likely that, below 260 °C, the increased reaction temperature promotes greater degrees of C-doping which in turn increases the catalytic activity. At reaction temperatures above 260 °C, however, the

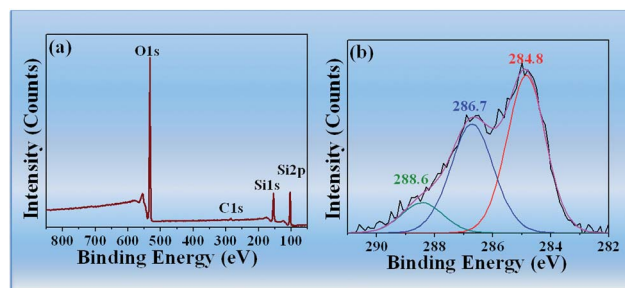


Fig. 4 (a) Broad-range XPS survey spectrum and (b) high-resolution C 1s XPS spectra of C-doped SiO<sub>2</sub> prepared at 260 °C and calcined at 600 °C.

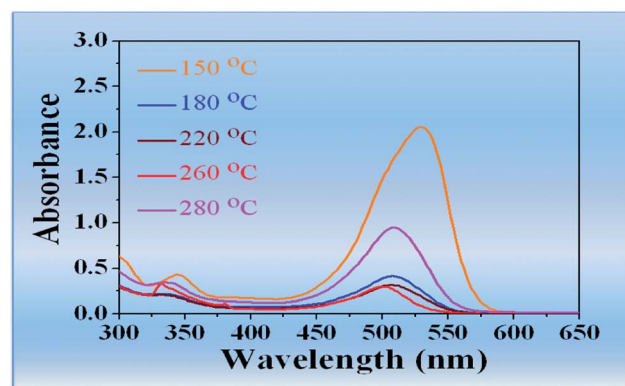


Fig. 5 Photocatalytic degradation of RhB by C-doped SiO<sub>2</sub> prepared at various temperatures.

rising C content is increasingly proportional to the concentration of oxygen vacancies, which, according to the photocatalytic theory, can become recombination centers for photo-produced holes and electrons,<sup>50</sup> leading to the decrease in photocatalytic activity. In addition, at higher reaction temperatures, larger particle sizes are generated which reduces the material's specific surface area, which in turn leads to fewer active sites and fewer substrate molecules to be adsorbed. As a result of all these factors, samples prepared by thermal treatment at 260 °C display the highest photocatalytic degradation efficiency.

The effects of post-thermal treatment on the photocatalytic activity of C-doped SiO<sub>2</sub> were also studied. Fig. 6(a) shows the effects of calcination at different temperatures on the photocatalytic activity of the prepared materials during degradation of RhB. These results demonstrate that increasing the calcination temperature from 600 to 1500 °C reduces the material's photocatalytic activity. This can be explained by noting that carbon bonded to the catalyst will be released as free carbon and will subsequently undergo oxidation with increasing calcination temperatures, which of course will reduce the C content of the lattice. This effect can be seen by comparing the XPS spectrum of the material calcined at 600 °C (Fig. 4(b)) with the material calcined at 1500 °C (Fig. 6(b)).

Our studies also indicated that other organic pollutants, such as methylene blue (MB) and methyl orange (MO), may be decomposed under near-UV irradiation using C-doped SiO<sub>2</sub>

(Fig. 7(a)). In addition, additional work showed that the SiO<sub>2</sub> material, because of its relatively high density, slow diffusion and high mobility, can be readily separated from the slurry mixture following the photocatalytic reaction. The SiO<sub>2</sub>, after being recycled and used for a total of ten RhB photodegradation trials, did not exhibit any significant loss of activity (less than 10%, Fig. 7(b)), indicating that the material was not photo-corroded during the photocatalytic oxidation of pollutant molecules in a neutral environment (pH = 7). Therefore, the C-doped SiO<sub>2</sub> synthesized in this work is sufficiently robust to be considered for applications as a photocatalyst in environmental purification on an industrial scale, when used in neutral solutions.

## Conclusions

It is well known that SiO<sub>2</sub> as a support is most commonly investigated for use in composite photocatalysts, because of its relative ease of preparation, good environmental stability and excellent compatibility with other materials. To the best of our knowledge, this is the first report of the near-UV-light photocatalytic activity of C self-doped SiO<sub>2</sub> samples. The formation of new energy states in this C-doped SiO<sub>2</sub> between the conduction band and the valence band is directly responsible for the reduction of the band gap and the material's associated photoactivity in conjunction with near-UV light. The synthesis of this material was designed such that it could be readily applied to industrial-scale processing, and included the use of low-cost, stable precursors and minimal production of undesirable byproducts. This one-step, environmentally friendly synthesis method may provide a new means of designing and synthesizing series of C-doped metal oxide semiconductors based on oxides such as TiO<sub>2</sub>, ZnO, MoO<sub>3</sub>, CeO<sub>2</sub>,  $\alpha$ -Fe<sub>2</sub>O<sub>3</sub>, ZrO<sub>2</sub>, WO<sub>3</sub> and SnO<sub>2</sub> for use in photo-assisted catalytic reactions. Furthermore, other non-metal elements, such as B, S, F and N, may also be doped into SiO<sub>2</sub> and may narrow the band gap sufficiently so as to shift the optical absorption of SiO<sub>2</sub> into the visible region. As a result of their low cost and potentially tunable properties, such materials should prove to be effective in future industrial applications related to pollution control and solar energy conversion.

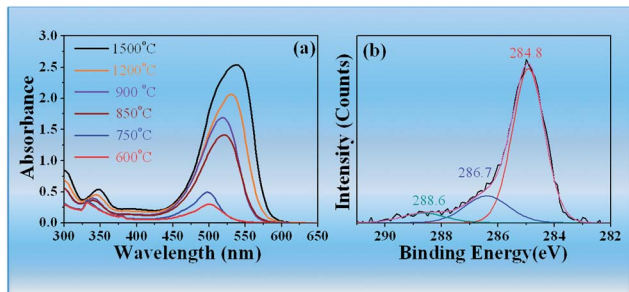


**Fig. 6** (a) Photocatalytic degradation of RhB by C-doped SiO<sub>2</sub> calcined at various temperatures and (b) high-resolution C 1s XPS spectra of C-doped SiO<sub>2</sub> samples prepared at 260 °C and calcined at 1500 °C.

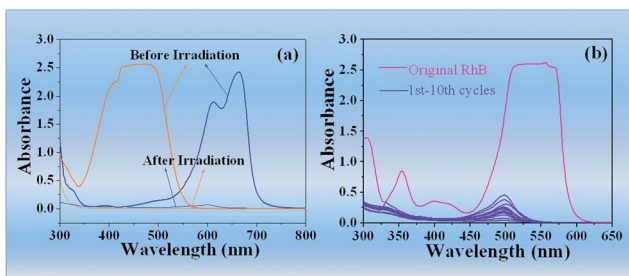


**Fig. 7** (a) UV-vis absorption spectra of methylene blue (blue line) and methyl orange (orange line) before and after irradiation for 3 h in the presence of the SiO<sub>2</sub>. The original concentration of solutions was 10<sup>-4</sup> M. (b) UV-vis absorption spectra of RhB solutions after photodecomposition following repeated trials with recycled C-doped SiO<sub>2</sub> samples.

## Acknowledgements

This work is supported by Hong Kong GRC grants 604710 and 605411.

## References

- 1 C. Allegre, M. Maisseu, F. Charbit and P. Moulin, *J. Hazard. Mater.*, 2004, **116**, 57–64.
- 2 V. Golob, A. Vinder and M. Simonič, *Dyes and Pigments*, 2005, **67**, 93–97.
- 3 A. Alinsafi, M. Khemis and M. N. Pons, *Chemical Engineering and Processing: Process Intensification*, 2005, **44**, 461–470.
- 4 M. Simonič and A. Lobnik, *Desalination*, 2011, **271**, 219–224.

- 5 Z. Y. Zhang, I. M. O'Hara, G. A. Kent and W. O. S. Doherty, *Ind. Crops Prod.*, 2013, **42**, 41–49.
- 6 A. Aouni, C. Fersi, B. Cuartas-Urbe, A. Bes-Pia, M. I. Alcaina-Miranda and M. Dhahbi, *Desalination*, 2012, **297**, 87–96.
- 7 N. Uzal, L. Yilmaz and U. Yetis, *Sep. Sci. Technol.*, 2010, **45**, 331–338.
- 8 E. Alventosa-deLara, S. Barredo-Damas, M. I. Alcaina-Miranda and M. I. Iborra-Clar, *J. Hazard. Mater.*, 2012, **209**, 492–500.
- 9 K. Tanaka, K. Padermpole and T. Hisanaga, *Water Res.*, 2000, **34**, 327–333.
- 10 N. Soltani, E. Saion, M. Z. Hussein, M. Erfani, A. Abedini, G. Bahmanrokh, M. Navasery and P. Vaziri, *Int. J. Mol. Sci.*, 2012, **13**, 12242–12258.
- 11 A. P. L. Batista, H. W. P. Carvalho, G. H. P. Luz, P. F. Q. Martins, M. Gonçalves and L. C. A. Oliveira, *Environ. Chem. Lett.*, 2010, **8**, 63–67.
- 12 T. D. Nguyen-Phan and E. W. Shin, *J. Ind. Eng. Chem.*, 2011, **17**, 397–400.
- 13 S. Khanchandani, S. Kundu, A. Patra and A. K. Ganguli, *J. Phys. Chem. C*, 2012, **116**, 23653–23662.
- 14 P. Y. Dong, Y. H. Wang, L. N. Guo, B. Liu, S. Y. Xin, J. Zhang, Y. R. Shi, W. Zeng and S. Yin, *Nanoscale*, 2012, **4**, 4641–4649.
- 15 P. A. Mangrulkar, V. Polshettiwar, N. K. Labhsetwar, R. S. Varma and S. S. Rayalu, *Nanoscale*, 2012, **4**, 5202–5209.
- 16 Y. Yamada, M. Mizutani, T. Nakamura and K. Yano, *Chem. Mater.*, 2010, **22**, 1695–1703.
- 17 S. I. Cha, K. H. Hwang, Y. H. Kim, M. J. Yun, S. H. Seo, Y. J. Shin, J. H. Moon and D. Y. Lee, *Nanoscale*, 2013, **5**, 753–758.
- 18 H. Yang and Z. H. Liu, *Cryst. Growth Des.*, 2010, **10**, 2064–2067.
- 19 S. Senapati, S. K. Srivastava and S. B. Singh, *Nanoscale*, 2012, **4**, 6604–6612.
- 20 C. Harris and P. V. Kamat, *ACS Nano*, 2010, **4**, 7321–7330.
- 21 K. Girija, S. Thirumalairajan, A. K. Patra, D. Mangalaraj, N. Ponpandian and C. Viswanathan, *Semicond. Sci. Technol.*, 2013, **28**, 035015.
- 22 S. Sakthivel, S. U. Geissen, D. W. Bahnemann, V. Murugesan and A. Vogelpohl, *J. Photochem. Photobiol., A*, 2002, **148**, 283–293.
- 23 Q. Wei, Z. Zhang, Z. Li, Q. Zhou and Y. Zhu, *J. Phys. D: Appl. Phys.*, 2008, **41**, 202002.
- 24 H. G. Yang, C. H. Sun, S. Z. Qiao, J. Zou, G. Liu, S. C. Smith, H. M. Cheng and G. Q. Lu, *Nature*, 2008, **453**, 638–644.
- 25 Q. J. Xiang and J. G. Yu, *J. Phys. Chem. C*, 2011, **115**, 7355–7363.
- 26 C. Z. Wen, H. B. Jiang, S. Z. Qiao, H. G. Yang and G. Q. Lu, *J. Mater. Chem.*, 2011, **21**, 7052–7061.
- 27 P. A. Thiam, *Catal. Commun.*, 2009, **10**, 1920–1924.
- 28 Y. Badr, M. G. A. El-Wahed and M. A. Mahmoud, *J. Hazard. Mater.*, 2008, **154**, 245–253.
- 29 M. A. Mahmouda, A. Poncherib, Y. Badrc and M. G. A. El-Wahed, *S. Afr. J. Sci.*, 2009, **105**, 299–303.
- 30 K. H. Chen, Y. C. Pu, K. D. Chang, Y. F. Liang, C. M. Liu, J. W. Yeh, H. C. Shih and Y. J. Hsu, *J. Phys. Chem. C*, 2012, **116**, 19039–19045.
- 31 N. Negishi, S. Matsuzawa, K. Takeuchi and P. Pichat, *Chem. Mater.*, 2007, **19**, 3808–3814.
- 32 K. H. Chen, Y. C. Pu, K. D. Chang, Y. F. Liang, C. M. Liu, J. W. Yeh, H. C. Shih and Y. J. Hsu, *J. Phys. Chem. C*, 2012, **116**, 19039–19045.
- 33 M. Q. He, D. Li, D. L. Jiang and M. Chen, *J. Solid State Chem.*, 2012, **192**, 139–143.
- 34 C. L. Pang, H. Cui and C. X. Wang, *CrystEngComm*, 2011, **13**, 4082–4085.
- 35 B. S. Zhuo, Y. G. Li, X. K. Zhang and A. C. Yang, *J. Mater. Sci. Eng. B*, 2010, **172**, 15–17.
- 36 Y. H. Ryu, Y. J. Tak and K. Yong, *Nanotechnology*, 2005, **16**, S370–S374.
- 37 I. Aharonovich and Y. Lifshitz, *Appl. Phys. Lett.*, 2007, **90**, 263109–263112.
- 38 S. A. Bagshaw, E. Prouzet and T. J. Pinnavaia, *Science*, 1995, **269**, 1242–1244.
- 39 J. P. Dacquin, J. Dhainaut, D. Duprez, S. Royer, A. F. Lee and K. Wilson, *J. Am. Chem. Soc.*, 2009, **131**, 12896–12897.
- 40 C. Belver, C. Adan and M. Fernandez-Garcia, *Catal. Today*, 2009, **143**, 274–281.
- 41 T. Watanabe, T. Takizawa and K. Honda, *J. Phys. Chem.*, 1977, **81**, 1845–1851.
- 42 C. W. Lai, Y. H. Hsiao, Y. K. Peng and P. T. Chou, *J. Mater. Chem.*, 2012, **22**, 14403–14409.
- 43 H. G. Will, P. L. Khoa, G. Jonathan, T. A. Tiffany and J. S. Michael, *Science*, 1997, **276**, 1826–1828.
- 44 F. Dong, S. Guo, H. Q. Wang, X. F. Li and Z. B. Wu, *J. Phys. Chem. C*, 2011, **115**, 13285–13292.
- 45 S. W. Liu, C. Li, J. G. Yu and Q. J. Xiang, *CrystEngComm*, 2011, **13**, 2533–2541.
- 46 F. Dong, H. Q. Wang and Z. B. Wu, *J. Phys. Chem. C*, 2009, **113**, 16717–16723.
- 47 C. Maillaro-Dupuy, C. Guillard and P. Pichat, *New J. Chem.*, 1994, **18**, 941–948.
- 48 J. M. Herrmann, *Catal. Today*, 1999, **53**, 115–129.
- 49 J. C. Ivey, G. Al-Sayyed and P. Pichat, *Environ. Sci. Technol.*, 1990, **24**, 990–996.
- 50 D. H. Wang, L. Jia, X. L. Wu, L. Q. Lu and A. W. Xu, *Nanoscale*, 2012, **4**, 576–584.